MARTIAN ROUGHNESS AT 15-M SCALE FROM RADAR STATISTICS. C. Grima[1], N. E. Putzig[2], B. A. Campbell[3], M. R. Perry[2], S. P. Gulick[1], R. C. Miller[1], A. T. Russell[2], K. M. Scanlan[4], G. Steinbrügge[5], D. A. Young[1], S. D. Kempf[1], G. Ng[1], D. Buhl[1], and D. D. Blankenship[1] [1]Institute for Geophysics, University of Texas at Austin, TX, USA, (cyril.grima@utexas.edu), [2]Planetary Science Institute, Lakewood, CO 80401, USA, [3]Center for Earth and Planetary Studies, Smithsonian Insitution, Washington, DC 20569, USA, [4]Technical University of Denmark: Kongens Lyngby, Hovedstaden, DK , [5]Jet Propulsion Laboratory, Pasadena, CA, USA.

Introduction. Over the last decade the Mars' interior has been actively probed using orbital radar sounders to unveil the planet's subsurface morphology [1, 2]. However, radiometry of the planet's surface return has been underused even though it is rich in information regarding the surface composition and its roughness at wavelength (metric to decametric) scales suitable for fine geologic interpretation and landing site reconnaissance [3]. However, quantitatively deconvolving those contributions from the surface echo strength is usually ambiguous without the support of other observation sources. We report a roughness approximation methodology from the application of the Radar Statistical Reconnaissance (RSR) technique [4, 3] to the surface echo strength of the Shallow Radar (SHARAD) data [5]. SHARAD transmits a 10-MHz bandwidth centered at 20 MHz (λ = 15 m) [1], and has been in operation aboard NASA's Mars Reconnaissance Orbiter (MRO) since 2006. The studied region covers longitudes 135°E to 165°E and latitudes 5°S to 15°N. This region has been chosen because it locally includes most of the 30-dB-wide spectra of SHARAD reflectivity that can be observed planet-wide [4]. The region includes a range of weakly reflective terrains including Medusa Fossae Formation outliers and scattered Noachian rises, moderately bright Hesperian Elysium shield, as well as the middle-to-late Amazonian Cerberus plain that accounts for one of the brightest regions on Mars at SHARAD wavelength.

Surface Echo Statistics. It can be demonstrated that the total strength of the surface echo is composed of coherent energy (or reflectance, P_c) and incoherent energy (or scattering, P_n), so that the total power received is $P_t = P_c + P_n$ [e.g., 6]. P_c is modulated by the deterministic structure of the ground (e.g., composition, layering). P_n is modulated by the non-deterministic structure (roughness, near-surface heterogeneity like blocks or voids) and varies with the degree of disorganization and dimension of the elements making up the target at radar scales. The RSR technique is a methodology to deconvolve P_c and P_n from the random behavior of the surface return amplitude [4, 7]. It is an improvement over other reflectometry techniques that usually derive dimensionless parameters, without strict quantitative bounds to near-surface properties [8, 9].

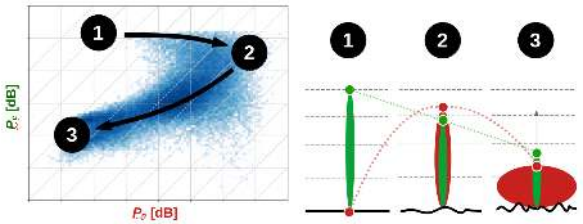

Figure 1: (Left) Distribution of the measured surface echoes in the $P_c - P_n$ space (axis scale on Fig. 2). (Right) Sketches illustrating three regimes depicting the relative evolution of P_c (green) and P_n (red) with increasing surface roughness for a nadir-looking radar.

Application. The signal gain is corrected for the effect of solar arrays (SA) and high-gain antenna (HGA) configuration following Campbell et al. [10]. Rolled observations have not been considered because the radiation pattern of the antenna is poorly known and the related gain variations cannot be assessed accurately. The behavior of the distribution in the 2-D $P_c - P_n$ space (Fig. 1. Left) exhibits a noteworthy comma-like shape that we aim at interpreting in the framework of signal growth with increasing surface roughness. When roughness increases from a flat surface (regime 1) to a very rough surface with quasi-isotropic scattering properties (regime 3), the coherent power diminishes. The power lost is thereby progressively transferred into the pool of incoherent energy, so that the incoherent power integrated over the half-space above the surface grows continuously with roughness. However, the incoherent energy that is intercepted by the antenna at normal incidence does not exhibit monotonic behavior. Incoherent energy first grows with roughness around the specular direction. But then, when the tilted elements making the surface pass a threshold depicted by regime 2, the integrated growth of the incoherent power tends to be concentrated in off-nadir directions and, counter-intuitively, the incoherent power intercepted by the antenna around the normal diminishes [11], going from regime 2 to regime 3. This dynamic is further illustrated by the precipitous drop in coherent power between regime 1 and 2 since P_c and P_n evolve in an opposite manner. After regime 2, the coherent fraction nearly stabilizes or even slightly increases, as both P_c and P_n shrink.

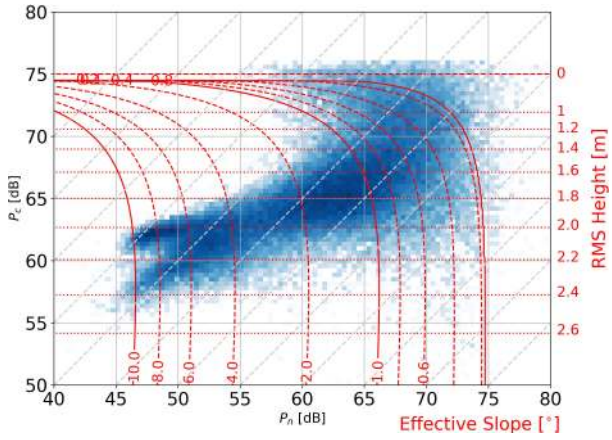

Figure 2: Parametrized roughness grid on top of the distribution of P_c and P_n retrieved over the studied area.

Roughness Approximation. The analytical relationships that bound the coherent and incoherent energies to the physical properties of the surface can be given by backscattering models. In general, at a given altitude z from the surface, at normal incidence, without volume scattering and for a stationary and ergodic surface, those components can be written in the form:

$$P_c = \alpha r^2 \chi(\sigma_h)^2 \quad (1)$$

$$P_n = \alpha r^2 L(z) \zeta(\sigma_h, l_c)^2 \quad (2)$$

where α is a calibration constant that can be adjusted so that P_c = 1 (or 0 dB loss) when the surface is a perfectly flat and conductive reflector (Fresnel coefficient r=1). r^2 is the Fresnel reflection coefficient in power; and $L(z)$ is the relative geometric propagation loss with respect to a specular reflection [4]. The surface roughness properties are defined by the root-mean-square (RMS) height (σ_h) and correlation length (l_c). The effective slope is given by $s_e = \sigma_h / l_c$ [12, 13]. $\chi(\sigma_h)^2$ and $\zeta(\sigma_h, l_c)^2$ are backscattering functions that are determined in this study by the Integral Equation Method (IEM) [14].

When the surface backscatter tends toward regime 1 for $P_{c_0} \approx 75\ dB$ in Fig. 1, the coherent energy is weakly affected by roughness and is mainly dependent on the surface permittivity through r^2. We use P_{c_0} as a reference for the surface echo strength reflected from a flat surface ($\sigma_h = 0$) with a given reflection coefficient r_0^2. A surface with the same r^2 that is affected by roughness will lose coherent energy with respect to P_{c_0} by a factor $\chi(\sigma_h)^2$. This allows for an association between the relative P_c and σ_h (Fig. 2). Each measurement is now associated to a ratio P_c/P_n and an RMS height (σ_h). Then, both can be injected into the ratio (1)/(2) to derive a correlation length. The obtained approximation for the surface roughness parameters is shown through the red grid on Fig. 2 and mapped on Fig. 3.

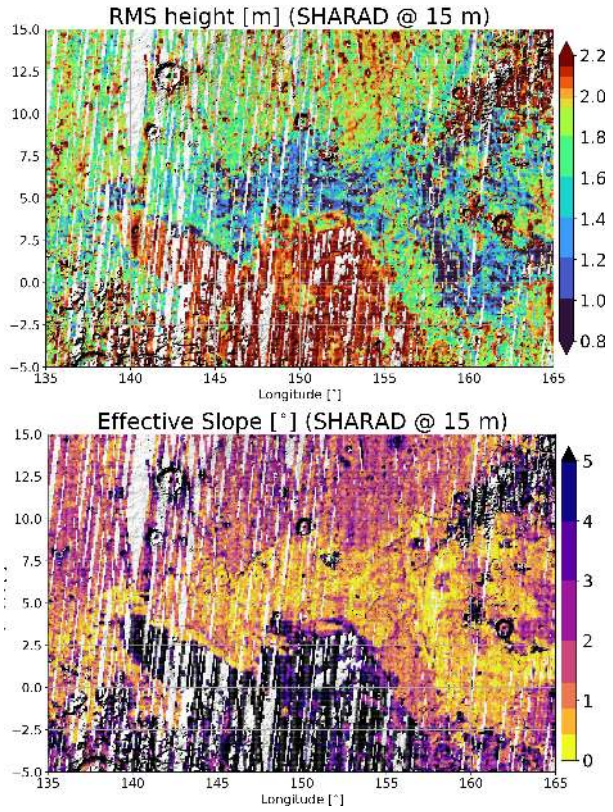

Figure 3: Derived roughness parameters

Discussion. This methodology provides quantitative metric-scale roughness information that may be used globally. We will further discuss at the conference the inherent assumptions, accuracy, and precision of the retrieved surface properties. Usage of this dataset for geologic interpretations are presented by Miller et al. [15] and Russell et al. [16].

References: **[1]** R. Croci et al., *Proceedings of the IEEE* 99 (2011), pp. 794–807. **[2]** R. Orosei et al., *PSS* 112 (2015), pp. 98–114. **[3]** C. Grima et al., *GRL* 41.19 (2014), pp. 6787–6794. **[4]** C. Grima et al., *Icarus* 220 (2012), p. 84. **[5]** R. Seu et al., *JGR* 112.E5 (2007). **[6]** F. T. Ulaby and D. G. Long. The University of Michigan Press, 2014. **[7]** C. Grima et al., *PSS* 103 (2014), pp. 191–204. **[8]** T. Hagfors, *Radio Sci.* 5 (1970), pp. 189–227. **[9]** B. A. Campbell et al., *JGR: Planets* 118 (2013), pp. 436–450. **[10]** B. A. Campbell et al., *Icarus* (2021), p. 114358. **[11]** F. T. Ulaby et al. Vol. 1-3. Addison-Wesley, Advanced Book Program, Reading, Massachusetts, 1981. **[12]** B. A. Campbell and J. B. Garvin, *Geophysical Research Letters* 20.9 (1993), pp. 831–834. **[13]** M. K. Shepard et al., *JGR* 106 (2001), pp. 32777–32796. **[14]** A. K. Fung and K. S. Chen, *IEEE Geoscience and Remote Sensing Letters* 1 (2004), p. 75. **[15]** R. Miller et al., *this conference* (2022). **[16]** A. Russell et al., *this conference* (2022).